Gastroenterology 2026;170:1000–1016

Activation of the Integrin αV-YAP-CTGF Axis in Liver Sinusoidal Endothelial Cells Promotes Liver Fibrogenesis, Leading to Portal Hypertension and Liver Carcinogenesis in Congestive Hepatopathy

Seiya Kato,[1] Hayato Hikita,[1,2] Osamu Tsukamoto,[3,4] Katsuhiko Sato,[1] Kohei Kamizono,[1] Yoichi Sasaki,[1] Kenji Fukumoto,[1] Yuta Myojin,[1] Kazuhiro Murai,[1] Yuki Tahata,[1] Yuki Makino,[1] Yoshinobu Saito,[1,2] Takahiro Kodama,[1] Daisuke Motooka,[5] Shogo Kobayashi,[6] Hideki Yokoi,[7,8] Masashi Mukoyama,[7] Yoshiaki Kubota,[9] Tomohide Tatsumi,[1] Hidetoshi Eguchi,[6] and Tetsuo Takehara[1]

[1]Department of Gastroenterology and Hepatology, Graduate School of Medicine, The University of Osaka, Osaka, Japan; [2]Integrated Frontier Research for Medical Science Division, Institute for Open and Transdisciplinary Research Initiatives (OTRI), The University of Osaka, Osaka, Japan; [3]Department of Medical Biochemistry, Graduate School of Medicine/Frontier Biosciences, The University of Osaka, Osaka, Japan; [4]Department of Medical Biochemistry, Hyogo Medical University, Hyogo, Japan; [5]NGS Core Facility, Bioinformatics Center, Research Institute for Microbial Diseases, The University of Osaka, Osaka, Japan; [6]Department of Gastroenterological Surgery, Graduate School of Medicine, The University of Osaka, Osaka, Japan; [7]Department of Nephrology, Kumamoto University Graduate School of Medical Sciences, Kumamoto, Japan; [8]Department of Nephrology, Kyoto University Graduate School of Medicine, Kyoto, Japan; and [9]Department of Anatomy, Keio University School of Medicine, Tokyo, Japan

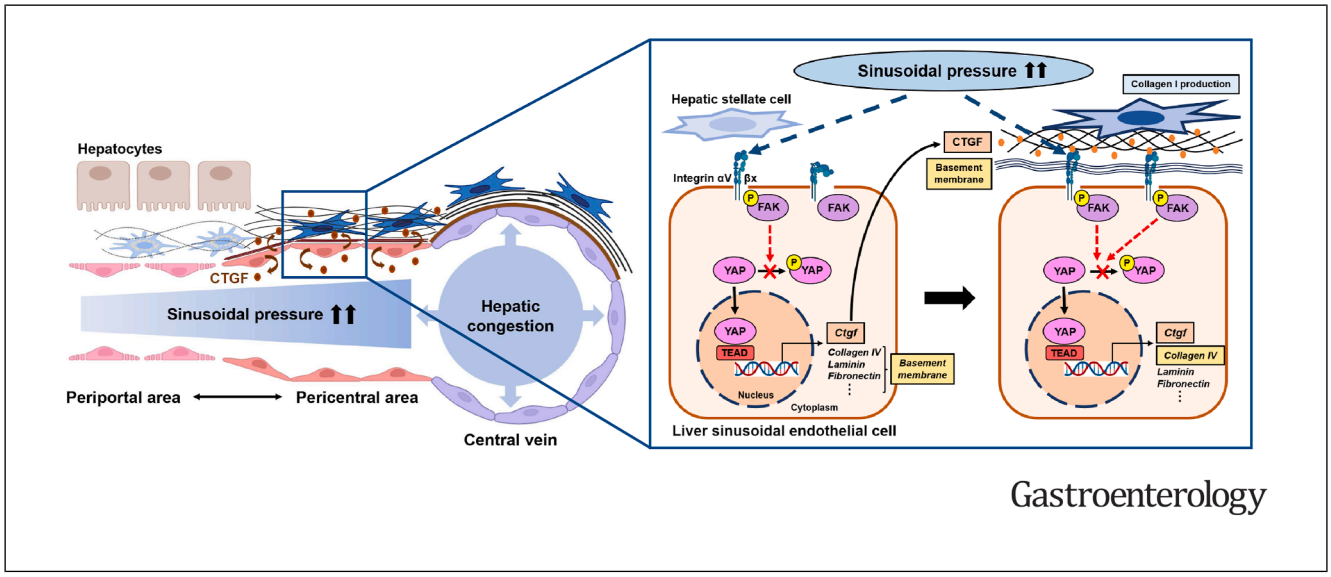

BACKGROUND & AIMS: Chronic liver congestion progresses to liver fibrosis, eventually leading to cirrhosis and cancer. This study aimed to elucidate the mechanism of congestive hepatopathy (CH), focusing on liver sinusoidal endothelial cells (LSECs). **METHODS:** Partial inferior vena cava ligation (pIVCL) was performed to induce hepatic congestion in mice. Single-cell RNA sequencing (scRNA-seq) was conducted on murine livers after pIVCL. Cells underwent hydrostatic pressure stimulation. scRNA-seq and spatial transcriptomics were performed on human livers from patients with Fontan-associated liver disease. **RESULTS:** The scRNA-seq analysis showed that the integrin signaling pathway and yes-associated protein (YAP) were activated in pericentral LSECs after pIVCL. The most upregulated gene in pericentral LSECs was connective tissue growth factor (CTGF). Hydrostatic pressure activated YAP through integrin αV, leading to the upregulation of CTGF and type IV collagen (COL4) expression in LSECs. LSEC-derived CTGF upregulated the type I collagen (COL1) and COL4 expression in hepatic stellate cells. CTGF knockout in endothelial cells ameliorated CH-induced liver fibrosis and portal hypertension and even suppressed liver tumorigenesis. Integrin αV inhibition alleviated CH-induced liver fibrosis and portal hypertension with the decreased expression of CTGF, COL4, and COL1. scRNA-seq and spatial transcriptomics of clinical Fontan-associated liver disease samples revealed YAP activation and CTGF upregulation in pericentral LSECs,

potentially leading to increased COL4 expression in LSECs and increased COL1 expression in hepatic stellate cells as fibrosis progressed. **CONCLUSIONS:** CTGF induction in LSECs may play an upstream role in the fibrogenesis of CH. The integrin αV–YAP–CTGF axis in LSECs could be a potential therapeutic target for CH.

Keyword: Mechanotransduction.

WHAT YOU NEED TO KNOW

BACKGROUND AND CONTEXT

The impact of liver sinusoidal endothelial cells on the pathogenesis of congestive hepatopathy has not been elucidated.

NEW FINDINGS

The activation of the yes-associated protein–connective tissue growth factor axis in liver sinusoidal endothelial cells through integrin αV contributes to the disease progression of congestive hepatopathy, such as liver fibrosis, portal hypertension, and liver carcinogenesis.

LIMITATIONS

The results of this study are based primarily on animal experiments and need to be validated in clinical practice.

CLINICAL RESEARCH RELEVANCE

The appropriate regulation of the integrin αV–yes-associated protein–connective tissue growth factor axis in liver sinusoidal endothelial cells offers novel therapeutic strategy for congestive hepatopathy. Inhibition of integrin αV-mediated yes-associated protein activation or connective tissue growth factor upregulation in liver sinusoidal endothelial cells could be a potential therapeutic strategy for patients with congestive hepatopathy such as Fontan-associated liver disease.

BASIC RESEARCH RELEVANCE

The integrin αV–yes-associated protein–connective tissue growth factor axis in liver sinusoidal endothelial cells was identified as a novel mechanism in response to pressure stimulation. The activation of this axis leads to the production of basement membrane components in liver sinusoidal endothelial cells themselves and collagen synthesis in hepatic stellate cells, contributing to liver fibrogenesis and portal hypertension in the mouse model of congestive hepatopathy.

Hepatic congestion is caused by a significant and persistent increase in hepatic venous pressure due to congenital heart disease, right-sided heart failure, Budd-Chiari syndrome, and other conditions; it leads to fibrosis around central veins and along sinusoidal walls in pericentral areas, progressing to bridging fibrosis from central veins to other central veins or to portal tracts, a pattern known as "inverse lobulation," without clear evidence of inflammation.[1–3] After a prolonged course, this process eventually leads to cirrhosis and liver tumors.[1–3] This type of liver injury is referred to as congestive hepatopathy (CH).[2] In particular, liver complications caused by Fontan surgery are referred to as Fontan-associated liver disease (FALD).[4,5] The Fontan procedure directs systemic venous blood to the lungs without passing through a ventricle in the setting of complex congenital heart defects, such as tricuspid atresia, pulmonary atresia, and a single ventricle.[6] Although this procedure has dramatically improved the prognosis of children with congenital heart disease, it causes chronic vena cava stasis, which can lead to congestive liver damage, ultimately leading to liver cirrhosis and hepatocellular carcinoma in adulthood.[4,5] The number of patients post-Fontan surgery is increasing, and long-term management after Fontan surgery is an unmet need.[7]

Liver sinusoidal endothelial cells (LSECs) are highly differentiated endothelial cells (ECs) composing liver sinusoidal walls; morphologically, LSECs exhibit fenestration in the cytoplasm and lack a basement membrane (BM).[8,9] These unique features allow the efficient exchange of oxygen and nutrients between sinusoids and hepatocytes.[8,9] LSEC capillarization precedes hepatic fibrosis, a process characterized by the loss of fenestrae and the appearance of a BM.[10] LSECs are constantly exposed to mechanical loads such as shear stress, stretching, and pressure stimulation and respond appropriately to these stimuli.[11] In addition, LSECs maintain homeostasis in the liver sinusoids in coordination with hepatic stellate cells (HSCs) through cell–cell interactions such as the secretion of paracrine factors.[12,13] Previous studies have shown that stretch-stimulated LSECs contribute to sinusoidal microthrombus formation, leading to the activation of HSCs.[14,15] However, the impact of mechano-stress responses, especially the response to pressure stimulation, of LSECs on CH pathology has yet to be fully elucidated.

Here, we investigated the role of LSECs in the pathogenesis of CH using a mouse model of CH and a hydrostatic pressure stimulation system for in vitro experiments. Using the mouse model and single-cell RNA sequencing (scRNA-seq) analysis, we identified connective tissue growth factor (CTGF) as one of the most upregulated genes in LSECs and found that the activation of the integrin αV–yes-associated protein (YAP)–CTGF axis in LSECs promoted liver pathogenesis under increased sinusoidal pressure. Using scRNA-seq and single-cell–based spatial transcriptomics, we also confirmed that the YAP−CTGF axis was activated in LSECs

Abbreviations used in this paper: **α-SMA, alpha-smooth muscle actin; BM, basement membrane; CH, congestive hepatopathy; COL1, type I collagen; COL4, type IV collagen; CTGF, connective tissue growth factor; FALD, Fontan-associated liver disease; HPS, hydrostatic pressure stimulation; HSCs, hepatic stellate cells; IL-6, interleukin-6; KO, knockout; LSECs, liver sinusoidal endothelial cells; pIVCL, partial inferior vena cava ligation; RT-qPCR, quantitative reverse-transcription polymerase chain reaction; scRNA-seq, single-cell RNA sequencing; STAT3, signal transducer and activator of transcription 3; TAZ, transcriptional coactivator with PDZ-binding motif; TEAD, TEA domain factors; YAP, yes-associated protein.**

Most current article

0016-5085
https://doi.org/10.1053/j.gastro.2025.11.014

in clinical liver specimens from patients with FALD. The present study revealed that the integrin αV–YAP–CTGF axis in LSECs in response to mechanical stress contributes to the development of liver pathogenesis through sinusoidal hypertension.

Materials and Methods

Cell Culture

TMNK-1 cells (JCRB/HSRRB Cell Bank),[16] a human liver EC line, and LX-2 cells (Merck Millipore, Darmstadt,

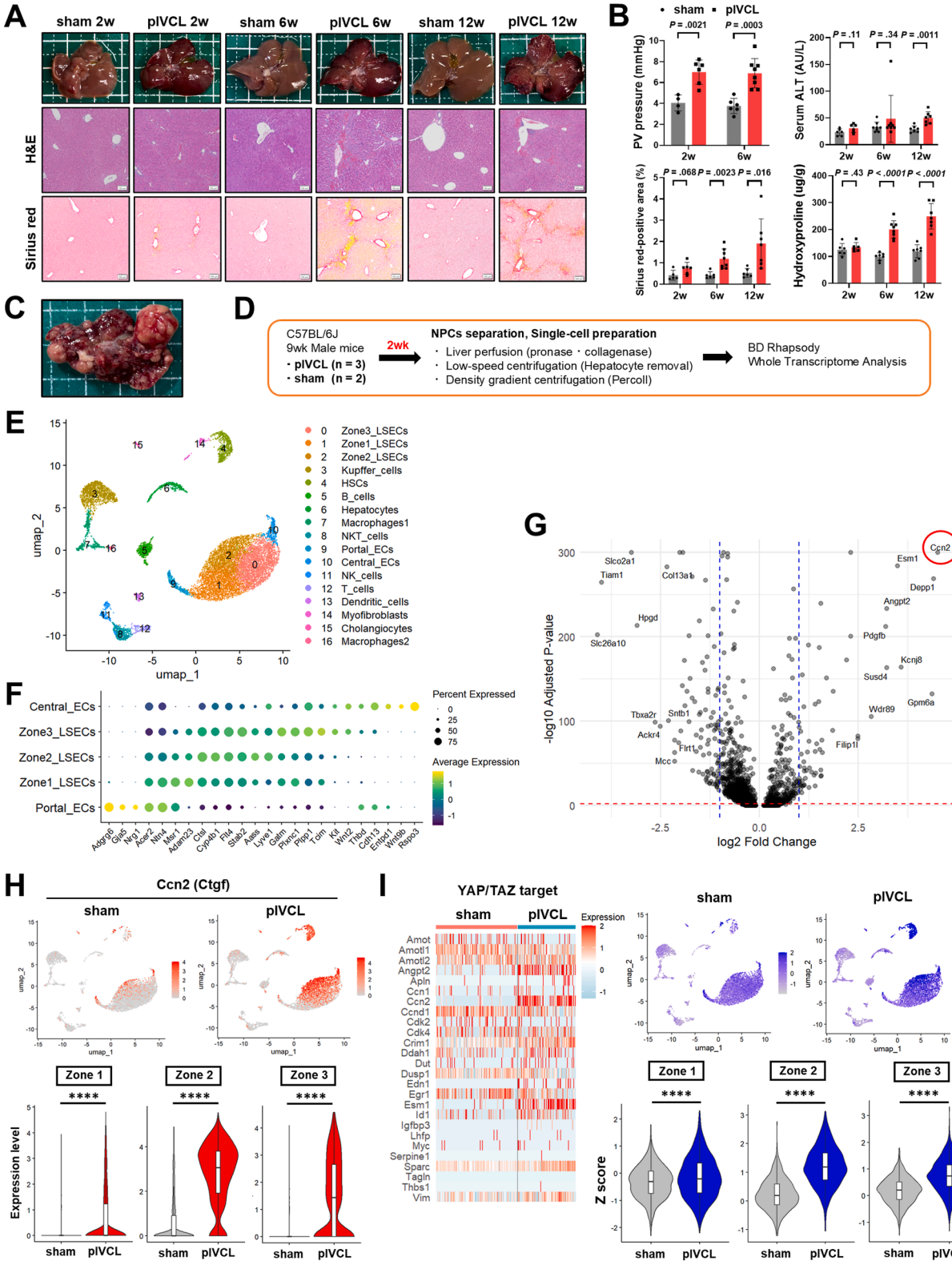

Germany),[17] a human HSC line, were cultured in Dulbecco's modified Eagle's medium at 37°C with 5% CO_2 (Sigma-Aldrich, St Louis, MO). The medium was supplemented with 10% fetal calf serum and 1% antibiotics (Thermo Fisher Scientific, Waltham, MA) unless otherwise indicated. All experiments were performed using cells with fewer than 20 passages. All in vitro and ex vivo experiments were performed at least twice, with similar results.

Primary Murine Liver Sinusoidal Endothelial Cells Isolation

Primary murine LSECs (mLSECs) were isolated from mice using the 2-step collagenase–pronase liver perfusion method and an immunomagnetic bead isolation protocol, as previously described with slight modifications.[18] Briefly, after a cell suspension was generated, hepatocytes were eliminated via low-speed centrifugation (50*g*), and dead cells and erythrocytes were eliminated via density gradient centrifugation using Percoll PLUS (GE17-5445-02; Cytiva, Tokyo, Japan). LSECs were selected using MACS CD146 MicroBeads (132-092-007; Miltenyi Biotec, Bergisch Gladbach, Germany). Purity was assessed using fluorescent acetylated–low-density lipoprotein (AcLDL) (5 μg/mL) (L23380; Thermo Fisher Scientific).[19] Briefly, after 20 min of incubation with AcLDL in serum-free medium, the proportion of cell that had taken up LDL was calculated via fluorescence-activated cell sorting (Canto II; Becton, Dickinson and Company, Franklin Lakes, NJ); the purity was >90% (Supplementary Figure 1*A* and *B*). mLSECs were cultured in endothelial cell basal medium 2 (PromoCell GmbH, Heidelberg, Germany) at 37°C with 5% CO_2. The medium was supplemented with 10% fetal calf serum and 1% antibiotics (Thermo Fisher Scientific) unless otherwise indicated. The cells were lysed for RNA or protein extraction. A list of the primers and antibodies used in this study is provided in Supplementary Tables 5 and 6.

Hydrostatic Pressure Loading Culture

mLSECs or TMNK-1 cells were exposed to hydrostatic pressure stimulation (HPS) as previously described, with slight modifications.[20] After incubation on a Collagen I-coated plate overnight, the cells were serum-starved for 6 hours and then exposed to periodic HPS for repeated cycles (0.01 Hz) between 101 and 135 kPa (absolute) for 8 hours using our original HPS system.[21] The system was maintained at 37°C in a CO_2 incubator (5% CO_2).

Mice

The generation of mice carrying 2 floxed CTGF alleles ($Ctgf^{fl/fl}$) was previously described.[22] The generation of transgenic mice expressing Cre^{ERT2} under the control of the VE-cadherin promoter sequence obtained from a bacterial artificial chromosome clone was previously described.[23] To generate EC-specific CTGF-deficient mice (*Cdh5-CreERT2* $Ctgf^{fl/fl}$; $Ctgf^{i\Delta EC}$), $Ctgf^{fl/fl}$ mice were crossed with heterozygous *Cdh5-CreERT2* transgenic mice. The generation of mice carrying 2 floxed YAP and transcriptional coactivator with PDZ-binding motif (TAZ) alleles ($Yap/Wwtr1^{fl/fl}$) was previously described.[24] In the same way, $Yap/Wwtr1^{fl/fl}$ mice were mated to generate EC-specific YAP/TAZ-deficient mice (*Cdh5-CreERT2* $Yap/Wwtr1^{fl/fl}$; $Yap/Wwtr1^{i\Delta EC}$). Littermates were used to compare phenotypes between the experimental groups. All the transgenic mice were generated in the C57BL/6 background. Only male mice were used in the experiments. The mice were housed under specific-pathogen-free conditions and had free access to water and standard mouse chow. All mice were provided humane care, and all experiments involving mice were approved by the Animal Care and Use Committee of Osaka University Medical School.

Partial Inferior Vena Cava Ligation

Male mice aged 8 to 10 weeks were subjected to partial inferior vena cava ligation (pIVCL) as previously described (Supplementary Figure 2*A* and *B*).[14] Briefly, the mice were anesthetized with 3 mixed anesthetic agents: 0.75 mg/kg medetomidine, 4 mg/kg midazolam, and 5 mg/kg butorphanol. After laparotomy, the suprahepatic inferior vena cava was circumferentially isolated and partially ligated with a steel wire (diameter, 0.6 mm). After the abdomen was closed, the effects of anesthesia were antagonized using 0.75 mg/kg medetomidine. The sham operation included all the preceding steps except for ligation. Detailed information about the scRNA-seq analysis is provided in the Supplementary Materials and Methods.

Portal Venous Pressure Measurement

Mice were anesthetized with 3 mixed anesthetic agents. After laparotomy, the portal vein was cannulated through the superior mesenteric vein, and portal pressure was measured directly by inserting a 1.2-Fr high-fidelity pressure catheter (Transonic Scisense, London, ON, Canada) (Supplementary

Figure 1. Partial inferior vena cava ligation elevates CTGF expression in pericentral LSECs. Wild-type male mice were subjected to pIVCL or sham surgery. (*A*) Representative images of livers and images of hematoxylin and eosin– and Sirius red–stained liver sections 2, 6, and 12 weeks after surgery (*scale bar*, 100 μm). (*B*) Portal venous (PV) pressure, serum alanine aminotransferase (ALT) levels, percent of Sirius red–stained area within liver sections and amount of hydroxyproline in the liver. n = 4–8/group. The data are shown as means ± SDs and were analyzed via 2-tailed Student *t* test. (*C*) Representative image of a liver with tumors formed 48 weeks after pIVCL. (*D–I*) scRNA-seq was performed on livers from the mice 2 weeks after surgery. Diagram of the scRNA-seq workflow (*D*). Uniform manifold approximation and projection (UMAP) plot of the 17 identified cell populations (*E*). EC populations were classified into portal ECs, central venous ECs and zone-specific LSECs (*F*). Differentially expressed genes in pericentral (zones 2 and 3) LSECs after pIVCL (PCT > 0.2) are shown in the volcano plot (*G*). UMAP distribution of *Ctgf* expression, and *Ctgf* expression in zone-specific LSECs (*H*). Heatmap of the expression of YAP/TAZ target genes in pericentral LSECs (*left*), UMAP distribution of the expression of the target genes (upper right), and *Z* scores for the expression of the target genes in zone-specific LSECs (*lower right*) (*I*). The data are shown as the median ± interquartile range (*H* and *I*). ****$P < .0001$ with the Mann-Whitney *U* test.

HEPATOBILIARY

Figure 2C).[25] The pressure was continuously monitored, and the average portal pressure was recorded using LabScribe4 software version 5.5.6 (ADInstruments, Colorado Springs, CO, Canada).

In Vivo Administration of a Pan-Integrin αV Inhibitor

Male mice aged 8 to 10 weeks were subjected to pIVCL, and after 2 weeks, Alzet osmotic pumps (Model No. 2004;

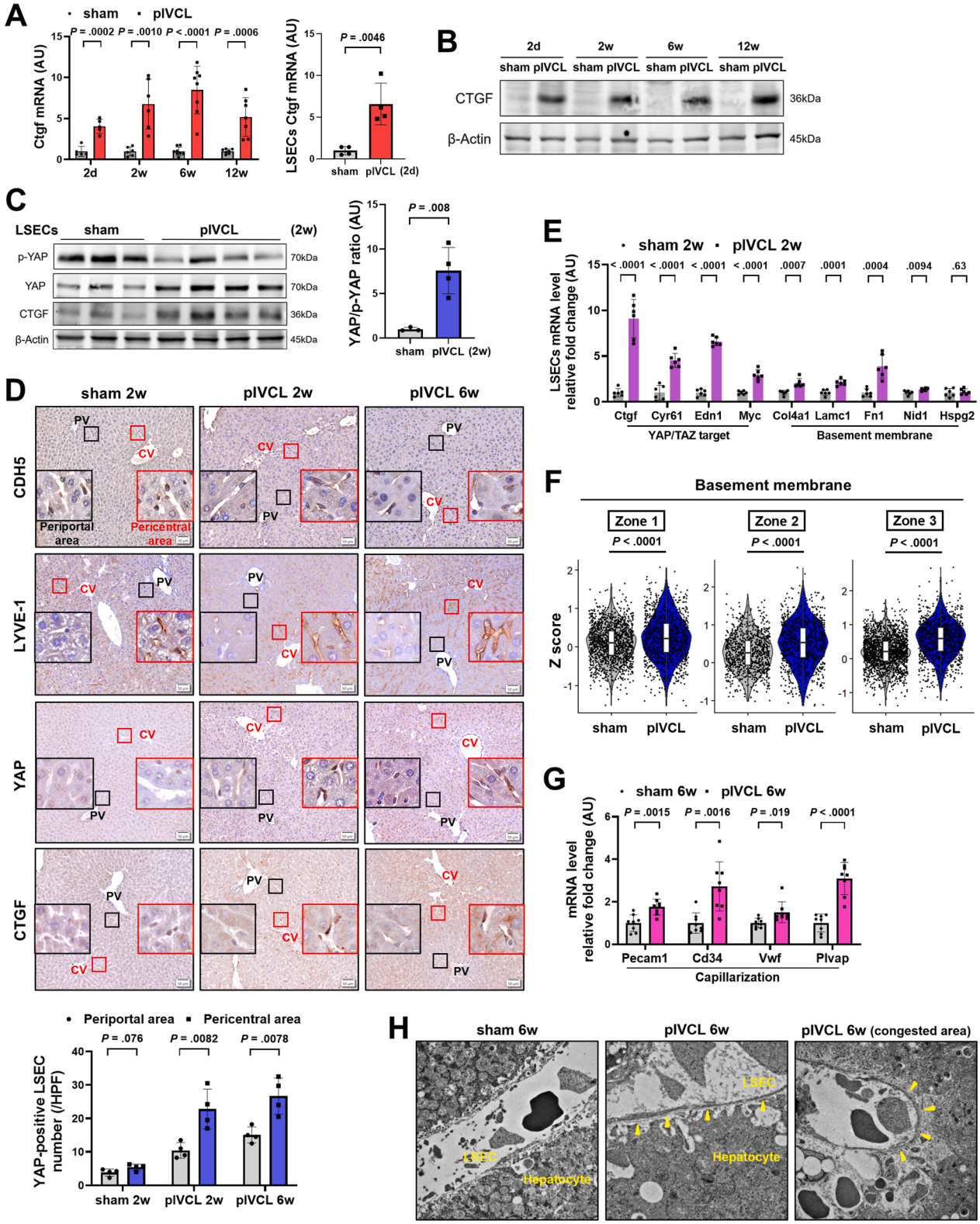

ALZET Osmotic Pumps, Cupertino, CA) containing either the pan-integrin αV inhibitor CWHM-12 (100 mg/kg/d) (HY-18644; MedChemExpress, Monmouth Junction, NJ) or vehicle (dimethyl sulfoxide) were inserted subcutaneously.[26]

Human Tissue Samples

Liver tissues were obtained from 15 patients with congestive liver diseases or normal livers for immunohistochemistry, Western blotting, quantitative reverse-transcription polymerase chain reaction (RT-qPCR), scRNA-seq, and spatial transcriptomics at Osaka University. Detailed information about the patients is provided in Supplementary Tables 1 and 2. All patients provided written informed consent, and the study was conducted in accordance with the principles of the Helsinki Declaration. The study protocol was approved by the Institutional Review Board (IRB) Committee at Osaka University Hospital (IRB No. 15267). Detailed information about the analysis of scRNA-seq and spatial transcriptomics is provided in the Supplementary Materials and Methods.

Statistical Analysis

Statistical analysis was performed using the 2-tailed Student *t* test or the Mann-Whitney *U* test to compare data between unpaired groups with parametric or nonparametric distributions, respectively. Ordinary 1- or 2-way analysis of variance followed by Sidak's multiple comparisons test was performed to compare parametric data among multiple groups. Otherwise, statistical analyses used are indicated in the figure legends. A P value $< .05$ was considered statistically significant. Prism, version 10.1.2 for Windows (RRID:SCR_002798; GraphPad Prism, San Diego, CA), was used for the analyses.

Results

Hepatic Congestion Due to Venous Obstruction Enhances Connective Tissue Growth Factor Expression in Pericentral Liver Sinusoidal Endothelial Cells in Mice

pIVCL in mice[14] induced portal hypertension and liver fibrosis, which was prominent in the pericentral areas, without evidence of an increase in alanine aminotransferase, well recapitulating CH in humans (Figure 1*A* and *B*). After pIVCL surgery, liver fibrosis progressed over time, and half of the mice (5 of 10) developed liver tumors with the characteristics of hepatocellular carcinoma 48 weeks after pIVCL (Figure 1*C* and Supplementary Figure 3*A*–*E*). scRNA-seq analysis of nonparenchymal-rich liver cells from the mice 2 weeks after pIVCL classified 13,749 cells into 17 clusters (Figure 1*D* and *E* and Supplementary Figure 4*A*–*C*), including 5 EC clusters: portal venous ECs, central venous ECs, and 3 specific LSECs for each hepatic zone (Figure 1*F*).[27] Considering that liver fibrosis occurs mainly in the pericentral areas, we examined the differentially expressed genes in pericentral (zones 2 and 3) LSECs. Among the 368 upregulated genes (PCT > 0.2, adjusted P value $< .05$) in the pericentral LSECs of the pIVCL group, connective tissue growth factor (*Ctgf*, also referred to as cellular communication network 2 [*Ccn2*]) was the most upregulated gene (Figure 1*G*, Supplementary Table 3). The increase in *Ctgf* expression was more pronounced in pericentral LSECs than in periportal (zone 1) LSECs (Figure 1*H*). Pathway and enrichment analyses revealed that the integrin signaling and focal adhesion pathways were activated in pericentral LSECs, suggesting that integrins are involved in mechano-stress responses as cell surface sensors (Supplementary Figure 5*A*).[28] The expression of target genes of YAP and TAZ (also known as WWTR1), known as major mechanotransducers,[29,30] was also increased in pericentral LSECs, as evaluated with *Z* scores (Figure 1*I*).

Hepatic Congestion Activates the Yes-associated Protein Signaling Pathway in LSECs and Induces LSEC Capillarization

CTGF expression in the liver and LSECs increased as early as 2 days and continued to increase until 12 weeks after pIVCL (Figure 2*A* and *B*). Immunofluorescence double staining confirmed that CTGF expression was upregulated in LSECs at 2 and 6 weeks after pIVCL (Supplementary Figure 6*A*). Western blotting suggested that the YAP signaling pathway was activated (Figure 2*C*). Immunohistochemistry revealed that YAP was expressed mainly in the nuclei of pericentral LSECs after pIVCL (Figure 2*D*). At 2 weeks after pIVCL, the expression of not only major YAP/TAZ target genes, such as *Ctgf*, *Cyr61*, *Edn1,* and *Myc,* but also BM-related genes, such as *Col4a1*, *Lamc1*, *Fn1,* and *Nid1,* was upregulated in isolated LSECs (Figure 2*E*). The scRNA-seq analysis results revealed that the expression levels of BM-related genes as well as YAP/TAZ target genes were greater in pericentral LSECs than in periportal LSECs

Figure 2. Hepatic congestion causes capillarization through upregulated CTGF expression and YAP activation in LSECs. Wild-type male mice were subjected to pIVCL or sham surgery and analyzed at the indicated time points after surgery. (*A*) *Ctgf* expression in whole livers and LSECs isolated from livers. n = 5–8/group. (*B*) Western blot images of CTGF in the liver. (*C*) Western blot images of phosphorylated YAP (p-YAP), YAP, and CTGF in isolated LSECs. The YAP/p-YAP ratio was calculated. n = 3–4/group. (*D*) Immunostaining images of CDH5, LYVE-1, YAP, and CTGF (*scale bar*, 50 μm). The number of YAP-positive cells per high-powered fields (HPFs). PV, portal vein; CV, central vein. (*E*) The expression of major YAP/TAZ target genes and BM-related genes in LSECs was analyzed via RT-qPCR. n = 6/group. (*F*) *Z* scores for the expression of BM-related genes in zone-specific LSECs. (*G*) The expression of capillarization marker genes in in whole livers. n = 8/group. (*H*) Transmission electron microscopy images of LSECs. The arrowheads indicate the development of the BM. The data are shown as means ± SDs, 2-tailed Student *t* test (*A, C, D, E,* and *G*). The data are shown as the median ± interquartile range, the Mann-Whitney *U* test (*F*).

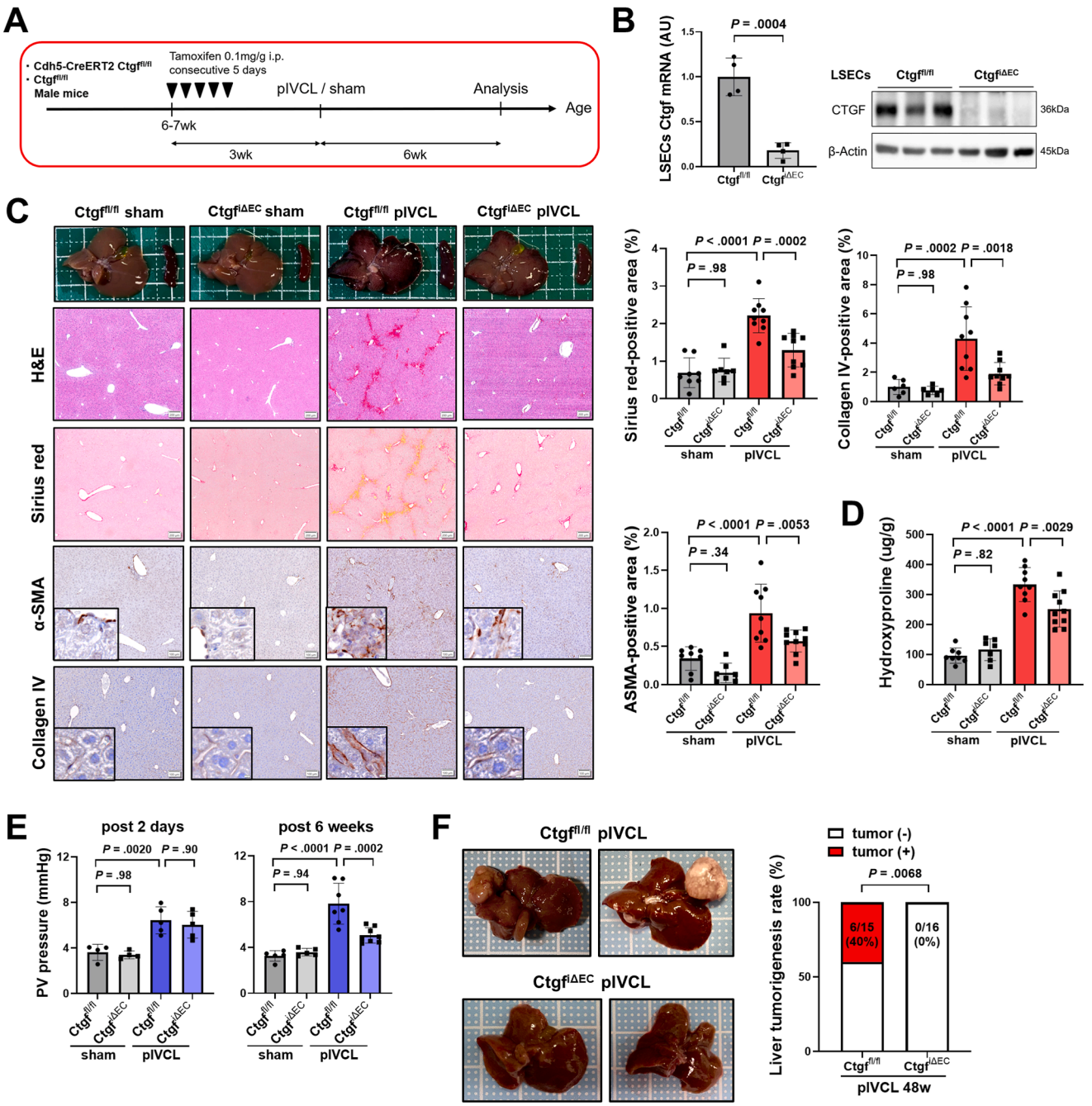

Figure 3. CTGF KO in LSECs suppresses liver fibrosis, portal hypertension, and liver tumorigenesis caused by hepatic congestion. Tamoxifen-induced endothelial cell–specific CTGF-KO mice (*Cdh5-CreERT2 Ctgf*$^{fl/fl}$; *Ctgf*$^{i\Delta EC}$) or control wild-type littermates (*Ctgf*$^{fl/fl}$) were subjected to pIVCL or sham surgery and analyzed 6 weeks or at the indicated time points after surgery. (*A*) Diagram of the experimental protocol. (*B*) CTGF expression in LSECs isolated from *Ctgf*$^{i\Delta EC}$ or *Ctgf*$^{fl/fl}$ mice 3 weeks after tamoxifen administration was analyzed via RT-qPCR and Western blotting. n = 3–4/group. (*C*) Representative images of livers, hematoxylin and eosin (H&E)-stained, Sirius red–stained, α-SMA–immunostained and collagen IV–immunostained liver tissue sections 6 weeks after surgery (*scale bar*, 100 μm). Percentage of Sirius red–, α-SMA–, and collagen IV–positive area in liver sections. n = 6–10/group. (*D*) The amount of hydroxyproline in the liver. n = 7–10/group. (*E*) Portal venous (PV) pressure levels 2 days and 6 weeks after surgery. n = 4–8/group. (*F*) Representative images of the liver of *Ctgf*$^{i\Delta EC}$ and *Ctgf*$^{fl/fl}$ mice and the liver tumorigenesis rate 48 weeks after pIVCL. n = 15–16/group. The data are shown as means ± SDs; two-tailed Student *t* test (*B*), 2-way analysis of variance followed by Sidak's multiple comparisons test (*C–E*) and Fisher's exact test (*F*).

(Figures 1*I* and 2*F*). In addition, at 6 weeks after pIVCL, the expression of capillarization marker genes such as *Pecam1*, *Cd34*, *Vwf,* and *Plvap* in the liver increased (Figure 2*G*). Transmission electron microscopy revealed the appearance of a BM in LSECs, which is a characteristic feature of LSEC capillarization (Figure 2*H*).

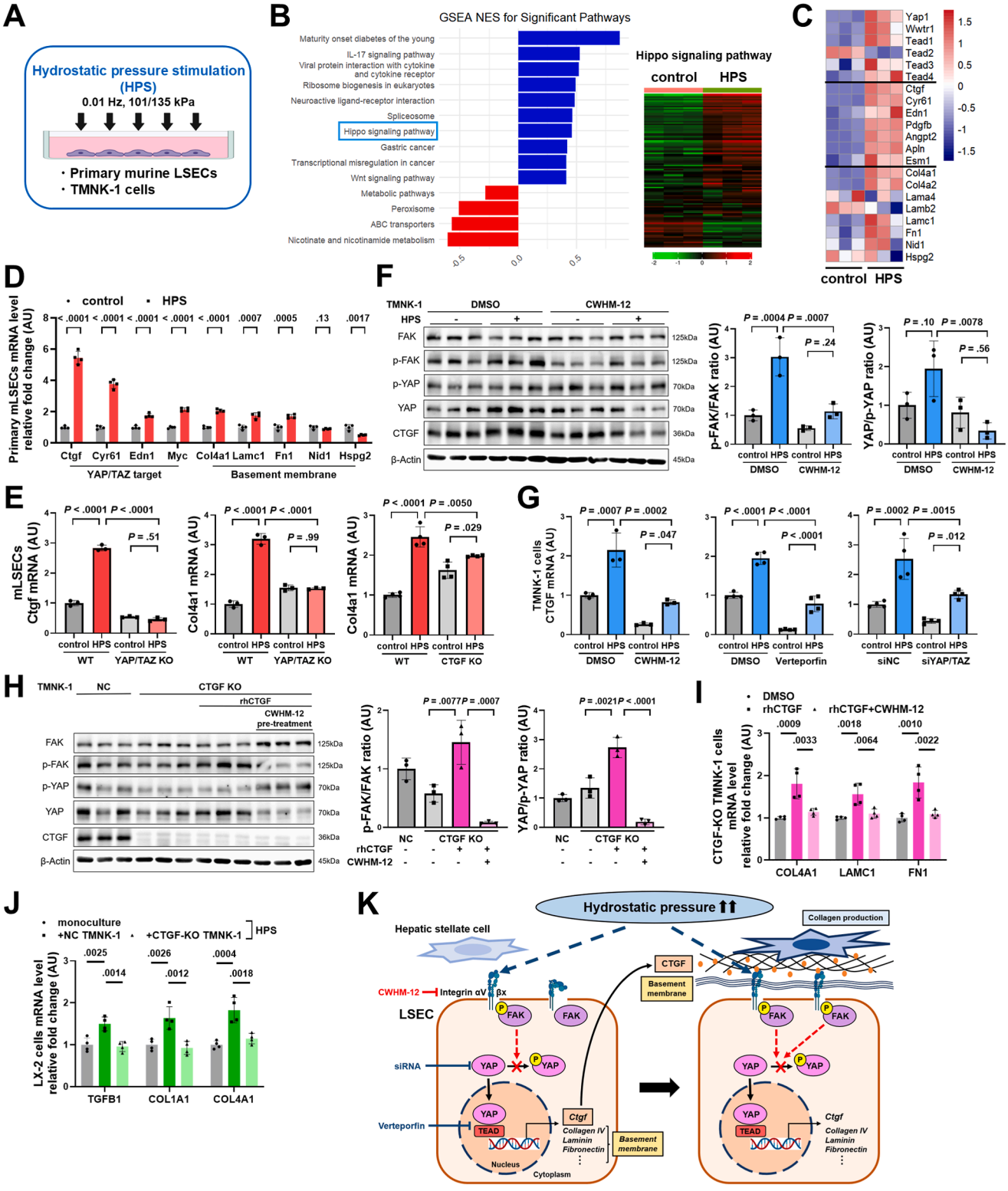

Connective Tissue Growth Factor Knockout in Liver Sinusoidal Endothelial Cells Suppresses Liver Fibrosis, Portal Hypertension, and Liver Tumorigenesis Caused by Hepatic Congestion

To examine the impact of CTGF in LSECs on pIVCL-induced CH, we performed pIVCL in $Ctgf^{i\Delta EC}$ mice (Figure 3*A*), in which CTGF expression in LSECs was lower than that in LSECs in control mice ($Ctgf^{fl/fl}$ mice) (Figure 3*B*). In the sham group, CTGF knockout (KO) in LSECs did not affect the phenotype. In the pIVCL group, CTGF KO in LSECs ameliorated pIVCL-induced pericentral fibrosis, as evidenced by reductions in Sirius red-, alpha-smooth muscle actin (α-SMA)-, type I collagen (COL1)A1- and collagen IV–positive areas (Figure 3*C* and Supplementary Figure 7*A*) and hydroxyproline levels in the liver (Figure 3*D*). After pIVCL, the expression of not only *Ctgf*, *Col1a1,* and *Col4a1* but also capillarization marker genes such as *Pecam1*, *Cd34,* and *Plvap*, and platelet endothelial cell adhesion molecule-1 (PECAM-1)–positive areas in the liver were significantly lower in $Ctgf^{i\Delta EC}$ mice than in $Ctgf^{fl/fl}$ mice (Supplementary Figure 7*B* and *C*). Transmission electron microscopy revealed that no distinct BM was observed between LSECs and hepatocytes in $Ctgf^{i\Delta EC}$ mice 6 weeks after pIVCL (Supplementary Figure 7*D*). scRNA-seq analysis also confirmed that CTGF KO in LSECs suppressed the upregulation of YAP/TAZ target genes and BM-related genes in LSECs (Supplementary Figure 8*A*–*F*). There was no significant difference in portal venous pressure at 2 days after pIVCL between $Ctgf^{i\Delta EC}$ and $Ctgf^{fl/fl}$ mice, and the pressure was significantly lower at 6 weeks after pIVCL in $Ctgf^{i\Delta EC}$ mice than in $Ctgf^{fl/fl}$ mice (Figure 3*E*). No liver tumorigenesis was observed in $Ctgf^{i\Delta EC}$ mice at 48 weeks after pIVCL (Figure 3*F*). In our previous study, we demonstrated that signal transducer and activator of transcription 3 (STAT3) and CTGF mutually activated each other via interleukin-6 (IL-6) family cytokine-mediated tumor-stroma crosstalk.[31] Consistently, in $Ctgf^{i\Delta EC}$ mice, the expression of IL-6 family cytokines and phosphorylation of STAT3 in the liver was suppressed (Supplementary Figure 9*A* and *B*).

Hydrostatic Pressure Stimulation Activates the YAP–CTGF Axis Through Integrin αV in LSECs, Resulting in the Upregulation of Basement Membrane-related Gene Expression

To mimic increased sinusoidal pressure due to vena cava stasis, mLSECs were subjected to HPS (Figure 4*A*). RNA sequencing analysis of HP-stimulated mLSECs revealed that the Hippo–YAP/TAZ signaling pathway was activated (Figure 4*B*). In mLSECs, HPS increased the expression of not only major YAP/TAZ target genes such as *Ctgf*, *Cyr61*, *Edn1,* and *Myc* but also BM-related genes such as *Col4a1*, *Lamc1,* and *Fn1* (Figure 4*C* and *D*). In mLSECs isolated from $Yap/Wwtr1^{i\Delta EC}$ mice, the HPS-induced upregulation of both *Ctgf* and *Col4a1* expression was completely suppressed (Figure 4*E*, left). In TMNK-1 cells, HPS activated integrin signaling and YAP, effects that were inhibited by pretreatment with the pan-integrin αV inhibitor CWHM-12 (Figure 4*F*). HPS-induced *CTGF* upregulation in TMNK-1 cells was suppressed by CWHM-12, verteporfin, a disrupter of YAP-TEAD (TEA domain factor) interactions, and short interfering RNA-induced silencing of YAP/TAZ (Figure 4*G*).

Connective Tissue Growth Factor Activates Yes-associated Protein Through Integrin αV as Positive Feedback in LSECs and Induces Collagen Synthesis in Hepatic Stellate Cells

To examine the impact of EC-derived CTGF on ECs themselves, we isolated mLSECs from $Ctgf^{i\Delta EC}$ mice. In mLSECs isolated from $Ctgf^{i\Delta EC}$ mice, the HPS-induced upregulation of *Col4a1* expression was partially suppressed (Figure 4*E*, right). HPS increased the expression of YAP/TAZ target genes such as *CYR61* and endothelin 1 (*EDN1*) in CTGF-KO TMNK-1 cells, suggesting that HPS-induced YAP activation is CTGF independent (Supplementary Figure 10*A*). Under conditions without hydrostatic pressure loading, recombinant human CTGF (rhCTGF) activated YAP and increased the expression of BM-related genes in CTGF-KO TMNK-1 cells. YAP activation and increased BM-related gene expression were suppressed by CWHM-12, an inhibitor of integrin αV, which is

Figure 4. HPS activates the integrin αV–YAP–CTGF axis in LSECs, resulting in the upregulation of BM-related gene expression. (*A*–*G*) Primary mLSECs and TMNK-1 cells were subjected to periodic HPS for 8 hours (n = 3–4/group). Diagram of the experimental protocol (*A*). RNA sequencing data of HP-stimulated mLSECs, including the top descriptions of pathways in the gene set enrichment analysis (GSEA) with normalized enrichment scores (NES) (left) (*B*), a heatmap of the expression of signature genes of the Hippo signaling pathway (right) (*B*), and a heatmap of the expression of downstream effectors of the Hippo signaling pathway, angiocrine factors, and BM-related genes (*C*). The expression of YAP/TAZ target genes and BM-related genes in HP-stimulated mLSECs (*D*). *Ctgf* and *Col4a1* expression in HP-stimulated LSECs isolated from tamoxifen-induced endothelial cell–specific YAP/TAZ knockout mice ($Yap/Wwtr1^{i\Delta EC}$) or control wild-type littermates ($Yap/Wwtr1^{fl/fl}$), and *Col4a1* expression in HP-stimulated LSECs isolated from $Ctgf^{i\Delta EC}$ or $Ctgf^{fl/fl}$ mice (*E*). Western blot images of focal adhesion kinase (FAK), phosphorylated FAK (p-FAK), phosphorylated YAP (p-YAP), YAP, and CTGF in HP-stimulated TMNK-1 cells with CWHM-12, a pan-integrin αV inhibitor (*F*). The p-FAK/FAK and YAP/p-YAP ratios were calculated. *CTGF* expression in HP-stimulated TMNK-1 cells treated with CWHM-12, verteporfin, a YAP inhibitor that disrupts YAP-TEA domain factor (TEAD) interactions, or YAP/TAZ short interfering RNA (siRNA) (*G*). (*H* and *I*) CTGF KO or negative control (NC) TMNK-1 cells were generated using the clustered regularly interspaced short palindromic repeat (CRISPR)-Cas9 system. Recombinant human CTGF (rhCTGF) was added to CTGF-KO TMNK-1 cells with or without CWHM-12 (n = 3–4/group). Western blot images of FAK, p-FAK, p-YAP, YAP, and CTGF (*H*). The p-FAK/FAK and YAP/p-YAP ratios were calculated. The expression of BM-related genes (*I*). (*J*) LX-2 cells were cocultured with CTGF-KO or NC TMNK-1 cells for 24 hours under HPS (n = 4/group). The expression of fibrosis-related genes in LX-2 cells. (*K*) Summary of in vitro studies. The data are shown as means ± SDs; 2-tailed Student *t* test (*D*) and 1-way (*H*–*J*) or 2-way (*E*–*G*) analysis of variance followed by Sidak's multiple comparisons test.

also known to interact with CTGF (Figure 4*H* and *I*).[32,33] These results suggest that not only HPS but also CTGF activates YAP.

Next, to examine the impact of EC-derived CTGF on HSCs, we cocultured LX-2 cells with CTGF-KO or control TMNK-1 cells in a transwell system under HPS. The

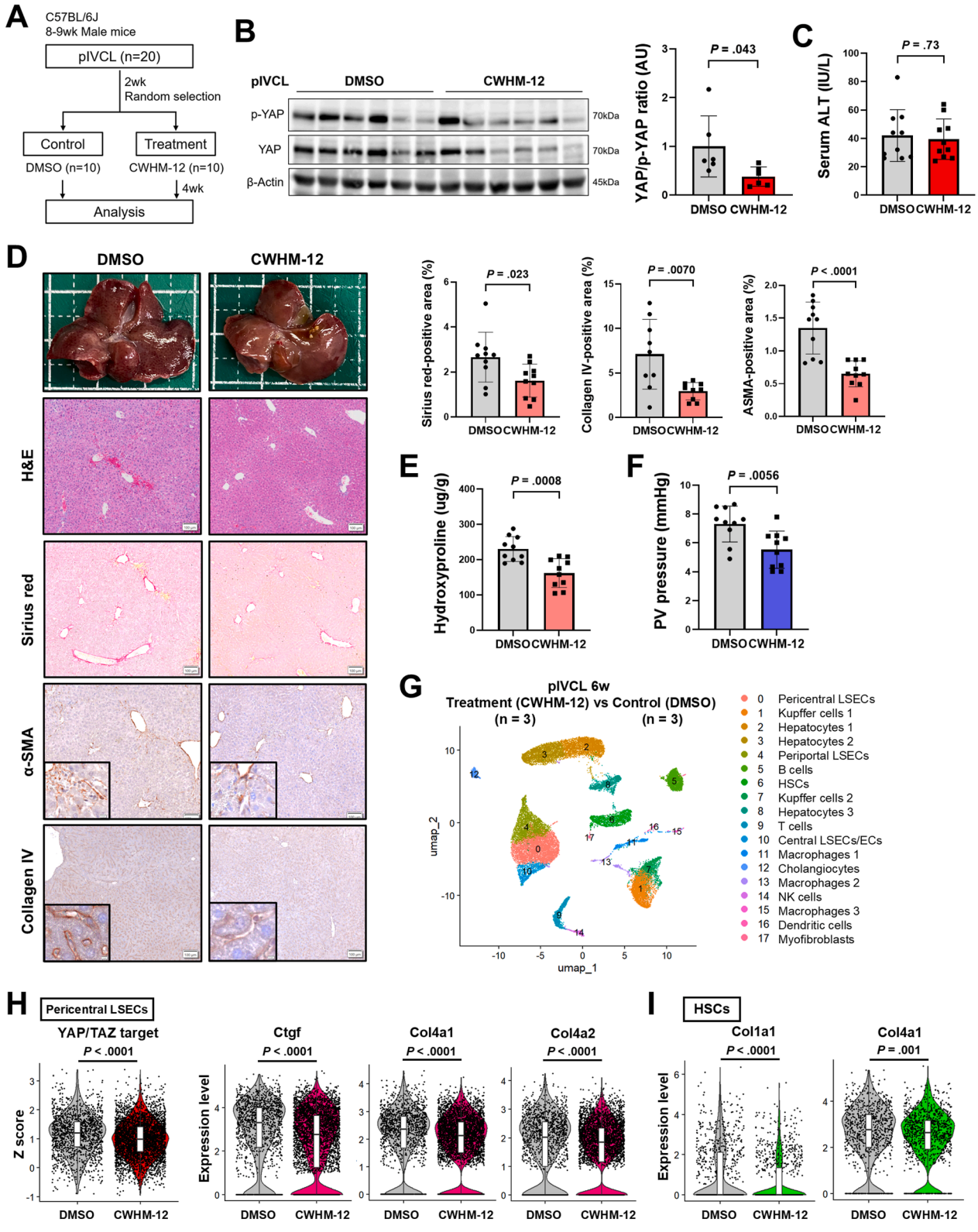

coculture of LX-2 cells with control TMNK-1 cells increased the expression of transforming growth factor-β1 (*TGFB1*), *COL1A1,* and *COL4A1* in LX-2 cells, effects that were counteracted when LX-2 cells were cocultured with CTGF-KO TMNK-1 cells (Figure 4*J*). In addition, rhCTGF increased the type 1 collagen-producing capacity and proliferative ability of LX-2 cells (Supplementary Figure 11*A* and *B*). To summarize the results of our in vitro experiments, HPS activated the integrin αV–YAP–CTGF axis in LSECs in combination with positive feedback, resulting in the upregulation of the expression of BM-related genes in LSECs and the promotion of collagen synthesis in HSCs (Figure 4*K*).

Administration of an Integrin αV Inhibitor Ameliorates Liver Sinusoidal Endothelial Cell Capillarization, Portal Hypertension, and Liver Fibrosis Caused by Hepatic Congestion in Mice

To explore the role of the integrin αV–YAP–CTGF axis as a potential therapeutic target in the pathogenesis of CH, CWHM-12 was administered to mice by continuous subcutaneous injection beginning 2 weeks after pIVCL for 4 weeks (Figure 5*A*). YAP activity in the liver was suppressed by CWHM-12 administration (Figure 5*B*). Although there was no difference in the serum alanine aminotransferase levels between the 2 groups (Figure 5*C*), the Sirius red-, α-SMA-, and collagen IV–positive areas and the hydroxyproline levels in the livers were significantly lower in the CWHM-12–treated mice than in the control mice (Figure 5*D* and *E*). CWHM-12 administration decreased the expression of *Tgfb1*, *Ctgf*, *Col1a1,* and *Col4a1*, as well as capillarization marker genes such as *Pecam1* and *Plvap* in the liver, the expression of COL1A1 in the liver, and the expression of CTGF in LSECs (Supplementary Figure 12*A*–*C*); it also significantly decreased portal venous pressure (Figure 5*F*). scRNA-seq analysis revealed that the expression levels of YAP/TAZ target genes, such as *Ctgf,* and BM-related genes, such as *Col4a1* and *Col4a2,* were lower in the pericentral LSEC cluster (cluster 0) of CWHM-12–treated mice than in those of control mice (Figure 5*G* and *H* and Supplementary Figure 4*D* and *E*). In the HSC cluster (cluster 6), *Col1a1* and *Col4a1* expression was also lower (Figure 5*I*).

Yes-associated Protein Activation and Upregulated CTGF Expression Are Observed in LSECs in the Livers of Patients With Fontan-associated Liver Disease

We analyzed normal liver and FALD liver samples via hematoxylin and eosin staining; Sirius red staining; and CTGF, integrin αV, and YAP immunostaining (Figure 6*A*). In the FALD samples, perisinusoidal fibrosis was evident in the areas of congestion (Figure 6*A*, left panels) and sinusoidal dilatation (Figure 6*A*, right panels). CTGF and integrin αV staining was present along the sinusoidal walls, and YAP staining was present mainly in the nuclei of liver sinusoidal cells (Figure 6*A*). Western blot results indicated YAP activation and higher CTGF and collagen IV expression in FALD livers than in normal livers (Figure 6*B*). RT-qPCR also revealed that *CTGF* expression was upregulated in the livers of patients with FALD (Figure 6*C*). The serum levels of N-terminal CTGF, which may be derived from fibrotic organs,[34] were also higher in FALD patients than in healthy controls (Figure 6*D*). In other types of CH such as congenital heart disease and Budd-Chiari syndrome, YAP activation in LSECs was also detected as in FALD (Supplementary Figure 13*A*). However, in other chronic liver diseases, such as viral hepatitis and steatohepatitis, YAP activation was less prominent than in CH (data not shown).

Next, we performed scRNA-seq analysis using livers from the FALD (n = 4) and normal (control, n = 3) groups, and 28,675 cells were classified into 9 clusters (Figure 6*E* and *F* and Supplementary Figure 14*A*–*C*). Among the 1002 upregulated genes (PCT > 0.1, adjusted *P* value < .05) in the EC cluster of the FALD livers, *CTGF* was the ninth most strongly upregulated gene (Figure 6*G* and *H* and Supplementary Table 4). Compared with the normal liver samples, in the FALD samples, in the EC cluster, the expression levels of YAP/TAZ target genes and BM-related genes were higher, and the integrin signaling and focal adhesion pathways were activated (Figure 6*I* and Supplementary Figure 15*A* and *B*); the expression of capillarization marker genes was also higher,

Figure 5. Administration of an integrin αV inhibitor ameliorates liver fibrosis and portal hypertension caused by hepatic congestion in mice. Wild-type male mice were subjected to pIVCL, and 2 weeks later, Alzet osmotic pumps containing either the pan-integrin αV inhibitor CWHM-12 (100 mg/kg/d) or vehicle (dimethyl sulfoxide [DMSO]) were inserted subcutaneously for 4 weeks. (*A*) Diagram of the experimental protocol. (*B*) Western blot images of phosphorylated YAP (p-YAP) and YAP. The YAP/p-YAP ratio was calculated. n = 6/group. (*C*) Serum alanine aminotransferase (ALT) levels. n = 10/group. (*D*) Representative images of livers and images of hematoxylin and eosin (H&E)-stained, Sirius red–stained, α-SMA–immunostained, and collagen IV–immunostained liver sections (*scale bar*, 100 μm). The percentages of Sirius red–positive area, α-SMA– and collagen IV–positive area were calculated. n = 9–10/group. (*E*) The amount of hydroxyproline in the liver. n = 10/group. (*F*) Portal venous (PV) pressure levels. n = 10/group. The data are shown as means ± SDs, 2-tailed Student *t* test (*B*–*F*). (*G*–*I*) scRNA-seq was performed on livers from the mice 6 weeks after pIVCL with or without CWHM-12 (n = 3/group). Uniform manifold approximation and projection (UMAP) plot of the 18 identified cell populations (*G*). The expression levels of YAP/TAZ target genes and *Ctgf*, *Col4a1*, and *Col4a2* expression levels were analyzed in pericentral LSECs (clusters 0) using *Z* scores (*H*). *Col1a1* and *Col4a1* expression levels in HSCs, cluster 6) (*I*). The data are shown as the median ± IQR, the Mann-Whitney *U* test (*H* and *I*).

whereas that of LSEC-specific marker genes was lower (Supplementary Figure 15*B*). Cell-cell interaction analysis via CellChat[35] revealed that the number of interactions in ECs was increased in FALD livers and that specific outgoing signals from ECs to other cells were increased through BM components (Supplementary Figure 15*C* and *D*).

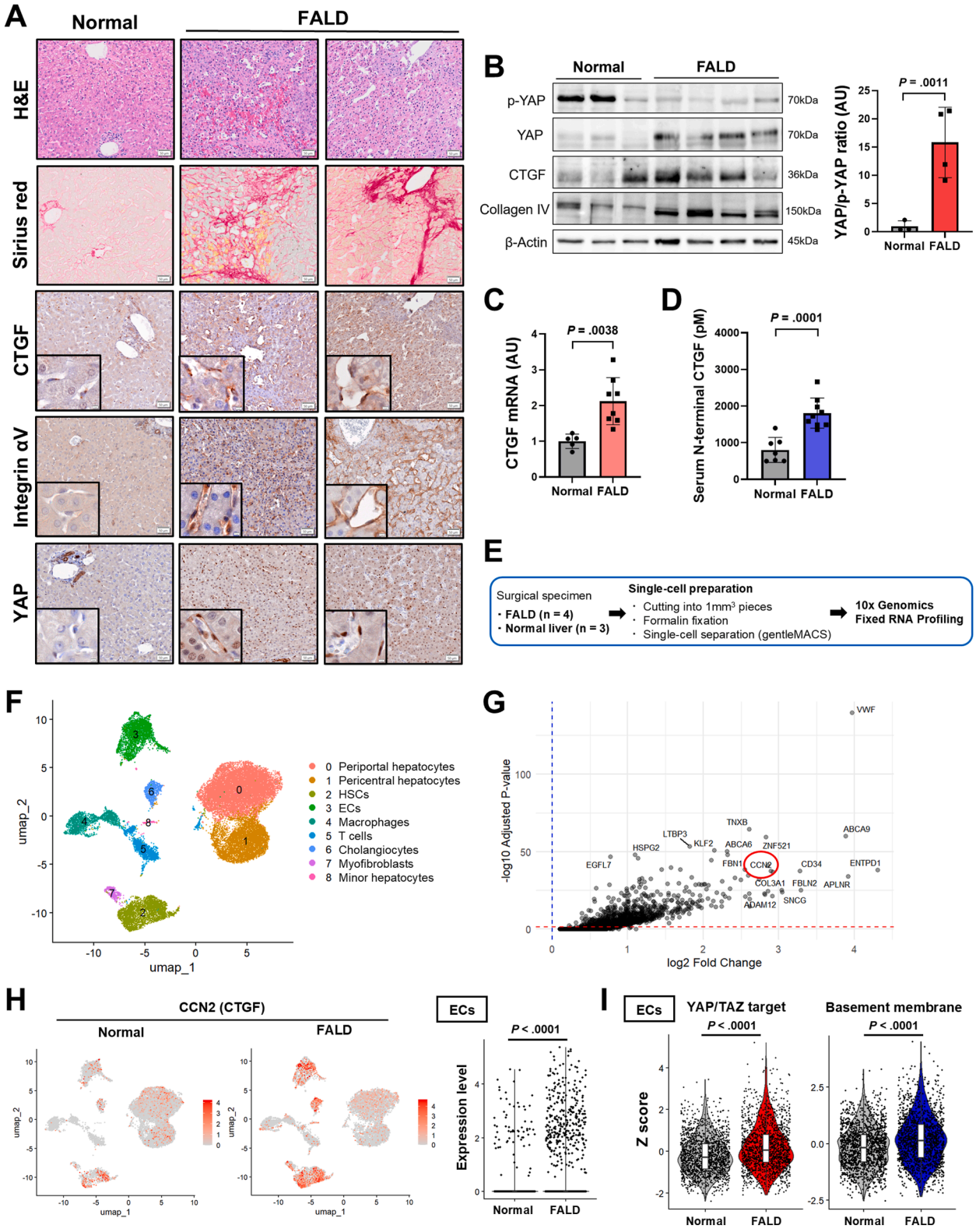

Spatial Transcriptomic Analysis Reveals the Fibrosis Progression Pattern via Differential Expression of Various Collagen Types in LSECs and HSCs in the Livers of Patients With Fontan-associated Liver Disease

Finally, we performed spatial transcriptomic analysis of 5 livers from patients with FALD and 2 normal livers at single-cell resolution using a CosMx Spatial Molecular Imager (Figure 7*A* and *B* and Supplementary Figure 16*A*–*C*). *CTGF* expression was detected in LSECs and HSCs in the FALD liver but was not prominent in the normal liver (Figure 7*C*), which was consistent with our scRNA-seq data (Figure 6*H*). Among LSECs in the FALD liver, *CTGF* expression was higher in pericentral LSECs than in periportal LSECs (Figure 7*D* and *E* and Supplementary Figure 16*D*). The expression of YAP/TAZ target genes was increased in pericentral LSECs in the FALD liver, as evaluated with Z scores (Figure 7*F*). In the FALD liver, type IV collagen (COL4) expression, including *COL4A1* and *COL4A2* expression, was notable in pericentral LSECs and HSCs, whereas COL1 expression, including *COL1A1* and *COL1A2* expression, was prominent in HSCs (Supplementary Figure 16*E*). Regarding fibrosis in the pericentral area in the FALD livers #1–3 (except for samples of severe cirrhosis, the FALD livers #4 and #5), we compared these gene expression levels between perisinusoidal fibrosis and bridging fibrosis (Figure 7*G* and Supplementary Figure 17*A*). In pericentral LSECs, CTGF expression was similarly high in both perisinusoidal and bridging fibrotic areas, whereas COL4 expression was significantly higher in bridging fibrotic areas (Figure 7*H* and Supplementary Figure 17*B*). In HSCs in the pericentral area, COL4 expression was not significantly different between perisinusoidal and bridging fibrotic areas, but COL1 expression was significantly higher in bridging fibrotic areas (Figure 7*I* and Supplementary Figure 17*C*), where the cell number was also increased (Supplementary Figure 17*D*). Given that fibrosis in CH begins as perisinusoidal fibrosis in the pericentral area and progresses to bridging fibrosis, the increased expression of CTGF in LSECs appears to occur at an early stage of the disease, followed by COL4 production from LSECs and COL1 production from HSCs, which lead to the development of bridging fibrosis.

Discussion

In the present study, we demonstrated in a mouse model and in a cell culture system that hepatic congestion led to YAP activation and YAP-dependent CTGF overproduction in LSECs, which play essential roles in liver fibrosis, portal hypertension, and liver tumorigenesis. Furthermore, single-cell analysis of human FALD samples revealed that YAP activation and increased CTGF expression in LSECs also occur in humans.

scRNA-seq analysis of livers from the CH mouse model, established via pIVCL, revealed that CTGF expression was most strongly upregulated in pericentral LSECs, which are located in the area where fibrosis first occurs in CH. CTGF is involved in cell adhesion and migration, angiogenesis, vascular permeability, and myofibroblast formation and activation; however, the role of CTGF varies based on context.[32,33,36] Our in vivo study revealed that CTGF KO in ECs attenuated pIVCL-induced liver fibrosis and portal hypertension, with decreased expression of COL1, a collagen type produced predominantly by activated HSCs. These findings suggest that CTGF induction in LSECs precedes COL1 deposition, indicating an upstream role in the fibrogenesis of CH. In addition, tumor formation was suppressed in EC-specific CTGF-KO mice, accompanied by the suppression of the expression of IL-6 family cytokines and the activation of STAT3 in the liver, suggesting that LSEC-derived CTGF potentially promotes liver carcinogenesis in CH via the amplification of IL-6 family cytokines.[31,37] Thus, LSEC-derived CTGF may be involved in the pathogenesis of a wider range of CH.

In patients with FALD, CTGF expression in the liver was markedly elevated, and the serum levels of its N-terminal fragment were increased. Our single-cell analyses of the FALD liver revealed that activation of YAP and high expression of CTGF were observed in LSECs. The significance of YAP signaling in liver disease is manifold.[38] YAP activation in hepatocytes is observed in patients with steatohepatitis and has been shown to contribute to liver fibrosis in a mouse model of steatohepatitis.[39] Activation of HSCs is accompanied by activation of YAP, which promotes hepatic fibrosis.[40] However, the significance of YAP in LSECs is unknown. We first demonstrated in the CH mouse model that YAP activation in LSECs occurred early in the pathogenesis of CH and contributed to HSC activation and LSEC capillarization via the YAP–CTGF axis. YAP activation in LSECs was observed not only in FALD but also in other

Figure 6. YAP activation and upregulated CTGF expression are present, as is an increase in BM expression, in LSECs in human FALD livers. (*A–C*) Samples from normal livers and FALD livers were analyzed. Representative images of hematoxylin and eosin (H&E)-stained, Sirius red–stained, and CTGF-, integrin αV–, and YAP-immunostained liver sections (*scale bar*, 50 μm) (*A*). *Left panel*: congested area. *Right panel*: sinusoidal dilatated area. Western blot images of p-YAP, YAP, CTGF, and collagen IV in the liver. n = 3–4/group (*B*). The YAP/p-YAP ratio was calculated. The expression of *CTGF* and *COL1A1* was analyzed via RT-qPCR. n = 5–8/group (*C*). (*D*) N-terminal CTGF levels were measured in sera from patients with FALD or healthy controls. n = 7–9/group. The data are shown as means ± SDs, 2-tailed Student *t* test (*B–D*). (*E–I*) scRNA-seq was performed on livers from FALD patients (n = 4) and healthy controls (controls) (n = 3). Diagram of the scRNA-seq workflow (*E*). Uniform manifold approximation and projection (UMAP) plot of the 9 identified cell populations (*F*). Volcano plot of differentially expressed genes in ECs in the FALD group (PCT > 0.1, upregulated genes) (*G*). UMAP distribution of *CTGF* expression (left) and *CTGF* expression in ECs (right) (*H*). *Z* scores for the expression of YAP/TAZ target genes and BM-related genes in ECs (*I*). The data are shown as the median ± interquartile range, the Mann-Whitney *U* test (*H* and *I*).

types of congestive liver disease. However, YAP activation in LSECs was not observed in a mouse model of carbon tetrachloride–induced liver fibrosis, and no improvement in liver fibrosis was produced by CTGF KO in ECs (Supplementary Figure 18*A*–*H*). Taken together, the mechanism of liver disease progression mediated by the YAP–CTGF axis in LSECs is characteristic of congestive liver diseases. Our study suggests that CTGF may serve not only

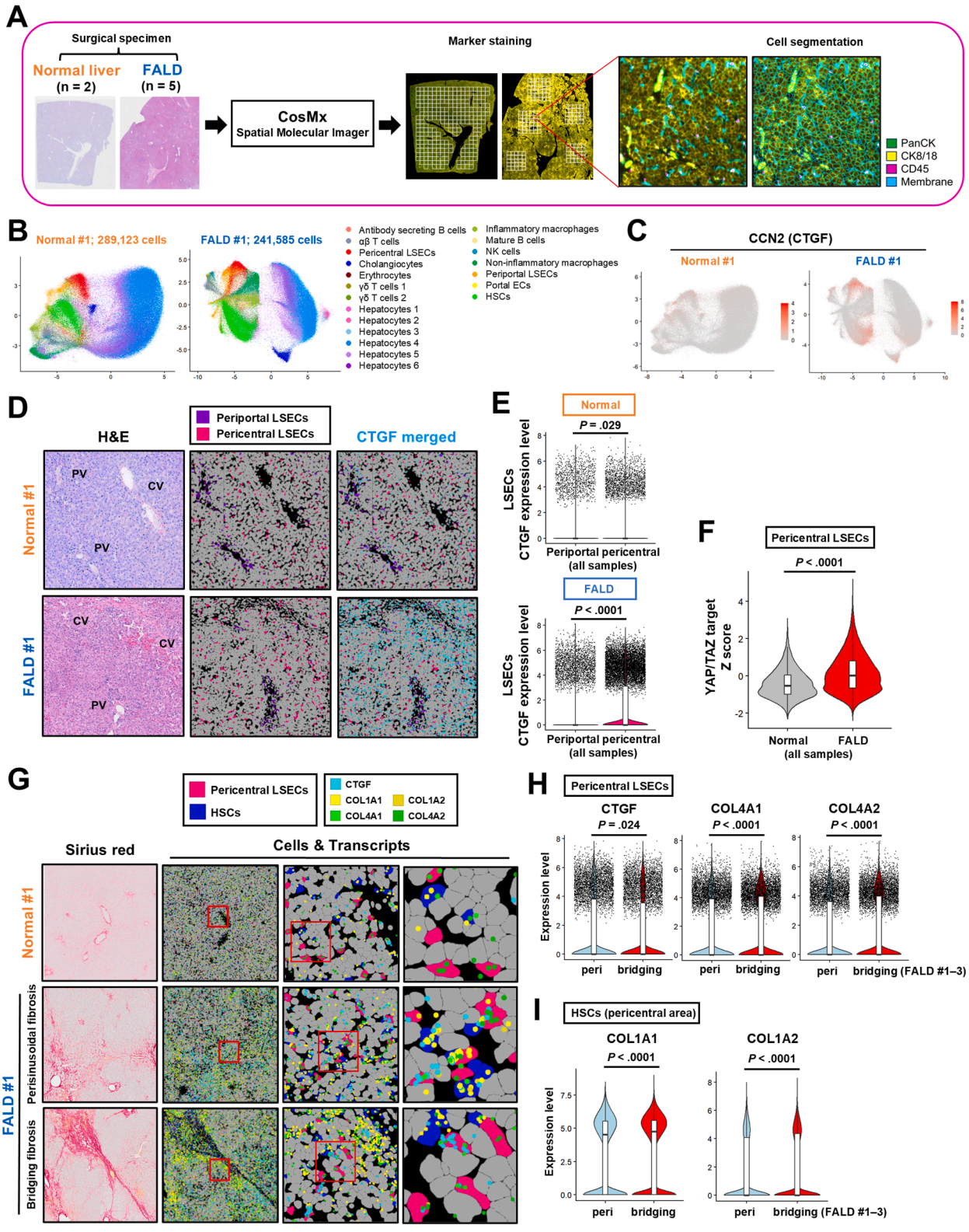

as a biomarker but also as a potential therapeutic target in CH such as FALD.

The present study revealed that LSECs expressed CTGF via YAP due to increased hydrostatic pressure. In general, YAP/TAZ, known to be downstream effectors of the Hippo signaling pathway, are key mechanotransducers, and the YAP/TAZ–TEAD pathway is important for the mechano-stress response.[30,41] The response of LSECs to mechanical stress such as shear stress or stretch stimulation has been examined.[15,42] However, the role of YAP/TAZ in the mechano-stress response in LSECs and their response to hydrostatic pressure have never been examined. The novel findings of our in vitro studies are that (1) HPS on LSECs promotes YAP-dependent CTGF and COL4 expression through integrin αV, (2) CTGF also activates YAP in LSECs through integrin αV, and (3) HP-stimulated LSECs induce collagen synthesis in HSCs, a process that is dependent on LSEC-derived CTGF. Given that COL4 expression was not sufficiently upregulated in EC-specific CTGF-KO mice and that the increase in COL4 expression caused due to hydrostatic loading was low in CTGF-KO LSECs, the expression of COL4 and other BM-related genes in LSECs and sinusoidal remodeling may not be sufficient by increased hydrostatic pressure alone and may require a feed-forward effect of CTGF.

The present study revealed that CTGF KO in ECs or integrin αV inhibition ameliorated pIVCL-induced liver fibrosis and portal hypertension with the decreased expression of COL4 and other capillarization markers. Portal hypertension is caused by LSEC capillarization, sinusoidal vasoconstriction, HSC activation, sinusoidal microthrombi, and other conditions.[15,43] COL4 is an essential component in BM formation during LSEC capillarization.[10,44] A previous study revealed that LSECs contributed to portal hypertension through COL4-driven sinusoidal remodeling in EC-specific COL4-KO mice.[44] Our scRNA-seq analyses of pIVCL-treated mice after CWHM-12 administration revealed that integrin αV inhibition suppressed YAP activation and the expression of CTGF and COL4 in LSECs, suggesting that the activation of the integrin αV−YAP−CTGF axis in LSECs plays a critical role in the pathological development of CH. Our study provides a proof of concept that integrin αV inhibition is a potential therapeutic target for CH. Inhibitors targeting integrin αV, such as small molecules and peptides, which have previously been developed, are being tested for some liver diseases, and have been shown to be generally safe and well tolerated.[45] In addition, therapeutic strategies targeting YAP and CTGF in LSECs using LSEC-specific delivery systems such as lipid nanoparticles are also promising.[46]

FALD is a newly conceptualized disease. The clinical features of FALD are becoming better understood,[4,5,7] although the cellular and molecular mechanisms underlying the pathogenesis of FALD remain unknown. Hu et al[47] analyzed FALD livers at the single-cell level, revealing unique interactions between central hepatocytes and HSCs, but did not analyze the features of ECs. Ma et al[48] revealed that LSEC-derived CXCL9 can recruit macrophages to the pericentral area in FALD livers, suggesting that a potential inflammatory response may contribute to the progression of FALD pathology. In our single-cell analysis of FALD livers, CTGF expression and YAP activation were observed in LSECs from the early stages of the disease, and the BM component of LSECs induced by CTGF was suggested to act on a variety of cells, including HSCs. Our study demonstrated that the pathogenesis of CH can progress not only through an inflammatory process but also through noninflammatory processes, independently of hepatocellular injury and inflammation. This study is limited by the small number of clinical samples; therefore, the accumulation and evaluation of FALD cases will be an important subject for future research.

In conclusion, in CH, mechano-stress in the liver sinusoids activates YAP and enhances CTGF expression in LSECs, potentially contributing to the development of liver fibrosis, portal hypertension, and, even more importantly, liver carcinogenesis. The appropriate regulation of the integrin αV–YAP–CTGF axis could be a potential therapeutic strategy for human CH.

Supplementary Material

Note: To access the supplementary material accompanying this article, visit the online version of *Gastroenterology* at www.gastrojournal.org, and at https://doi.org/10.1053/j.gastro.2025.11.014.

References

1. Giallourakis CC, Rosenberg PM, Friedmanet LS, et al. The liver in heart failure. Clin Liver Dis 2002;6:947–967.
2. Fortea JI, Puente Á, Cuadrado A, et al. Congestive hepatopathy. Int J Mol Sci 2020;21:9420.

Figure 7. Spatial transcriptomics revealed that CTGF expression is increased in pericentral LSECs in perisinusoidal fibrotic areas of human FALD livers. Single-cell spatial transcriptomic analysis was performed using livers from 5 FALD patients and 2 normal livers. (*A*) Diagram of the spatial transcriptomic analysis workflow. (*B*) Uniform manifold approximation and projection (UMAP) plot of the 20 identified cell populations. (*C*) UMAP distribution of *CTGF* expression. (*D*) Representative images of hematoxylin and eosin (H&E) staining, mapping images of periportal and pericentral LSECs, and mapping images showing the locations of *CTGF* mRNA (left). PV, portal vein; CV, central vein. (*E*) *CTGF* expression in periportal and pericentral LSECs (right). (*F*) *Z* scores of the expression of YAP/TAZ target genes in pericentral LSECs. (*G*) Representative images of Sirius red–staining and cell mapping images of pericentral LSECs and HSCs showing the mRNA locations of *CTGF*, *COL1*, and *COL4*. In the FALD liver, images of the pericentral area with perisinusoidal and bridging fibrosis. (*H*) The expression of *CTGF* and *COL4* in pericentral LSECs with perisinusoidal and bridging fibrosis of the FALD liver. (*I*) *COL1* expression in HSCs in the pericentral area with perisinusoidal and bridging fibrosis of the FALD liver. The data are shown as the median ± IQR, the Mann-Whitney *U* test (*E, F, H*, and *I*).

HEPATOBILIARY

3. Valla DC. Budd-Chiari syndrome/hepatic venous outflow tract obstruction. Hepatol Int 2018;12:168–180.
4. Gordon-Walker TT, Bove K, Veldtman G. Fontan-associated liver disease: a review. J Cardiol 2019; 74:223–232.
5. Hilscher MB, Wells ML, Venkatesh SK, et al. Fontan-associated liver disease. Hepatology 2022; 75:1300–1321.
6. Gewillig M. The Fontan circulation. Heart 2005; 91:839–846.
7. Emamaullee J, Zaidi AN, Schiano T, et al. Fontan-associated liver disease screening, management, and transplant consideration. Circulation 2020;142:591–604.
8. Poisson J, Lemoinne S, Boulanger C, et al. Liver sinusoidal endothelial cells: physiology and role in liver diseases. J Hepatol 2017;66:212–227.
9. Gracia-Sancho J, Caparrós E, Fernández-Iglesias A, et al. Role of liver sinusoidal endothelial cells in liver diseases. Nat Rev Gastroenterol Hepatol 2021; 18:411–431.
10. DeLeve LD. Liver sinusoidal endothelial cells in hepatic fibrosis. Hepatology 2015;61:1740–1746.
11. Tschumperlin DJ, Ligresti G, Hilscher MB, et al. Mechanosensing and fibrosis. J Clin Invest 2018; 128:74–84.
12. Deleve LD, Wang X, Guo Y. Sinusoidal endothelial cells prevent rat stellate cell activation and promote reversion to quiescence. Hepatology 2008;48:920–930.
13. Desroches-Castan A, Tillet E, Ricard N, et al. Bone morphogenetic protein 9 is a paracrine factor controlling liver sinusoidal endothelial cell fenestration and protecting against hepatic fibrosis. Hepatology 2019;70:1392–1408.
14. Simonetto DA, Yang HY, Yin M, et al. Chronic passive venous congestion drives hepatic fibrogenesis via sinusoidal thrombosis and mechanical forces. Hepatology 2015;61:648–659.
15. Hilscher MB, Sehrawat T, Arab JP, et al. Mechanical stretch increases expression of CXCL1 in liver sinusoidal endothelial cells to recruit neutrophils, generate sinusoidal microthombi, and promote portal hypertension. Gastroenterology 2019;157:193–209.
16. Matsumura T, Takesue M, Westerman KA, et al. Establishment of an immortalized human-liver endothelial cell line with SV40T and hTERT. Transplantation 2004; 77:1357–1365.
17. Xu L, Hui AY, Albanis E, et al. Human hepatic stellate cell lines, LX-1 and LX-2: new tools for analysis of hepatic fibrosis. Gut 2005;54:142–151.
18. Liu J, Huang X, Werner M, et al. Advanced method for isolation of mouse hepatocytes, liver sinusoidal endothelial cells, and Kupffer cells. Methods Mol Biol 2017; 1540:249–258.
19. Hammoutene A, Biquard L, Lasselin J, et al. A defect in endothelial autophagy occurs in patients with non-alcoholic steatohepatitis and promotes inflammation and fibrosis. J Hepatol 2020;72:528–538.
20. Miyashita Y, Tsukamoto O, Matsuoka K, et al. The CR9 element is a novel mechanical load-responsive enhancer that regulates natriuretic peptide genes expression. FASEB J 2021;35:e21495.
21. Yokoyama U, Tonooka Y, Koretake R, et al. Arterial graft with elastic layer structure grown from cells. Sci Rep 2017;7:140.
22. Toda N, Mori K, Kasahara M, et al. Crucial role of mesangial cell-derived connective tissue growth factor in a mouse model of anti-glomerular basement membrane glomerulonephritis. Sci Rep 2017;7:42114.
23. Okabe K, Kobayashi S, Yamada T, et al. Neurons limit angiogenesis by titrating VEGF in retina. Cell 2014; 159:584–596.
24. Reginensi A, Scott RP, Gregorieff A, et al. Yap- and Cdc42-dependent nephrogenesis and morphogenesis during mouse kidney development. PLoS Genet 2013;9: e1003380.
25. Ikenaga N, Liu SB, Sverdlov DY, et al. A new Mdr2(−/−) mouse model of sclerosing cholangitis with rapid fibrosis progression, early-onset portal hypertension, and liver cancer. Am J Pathol 2015;185:325–334.
26. Henderson NC, Arnold TD, Katamura Y, et al. Targeting of alphav integrin identifies a core molecular pathway that regulates fibrosis in several organs. Nat Med 2013; 19:1617–1624.
27. Su T, Yang Y, Lai S, et al. Single-cell transcriptomics reveals zone-specific alterations of liver sinusoidal endothelial cells in cirrhosis. Cell Mol Gastroenterol Hepatol 2021;11:1139–1161.
28. Sun Z, Guo SS, Fässler R. Integrin-mediated mechanotransduction. J Cell Biol 2016;215:445–456.
29. Kim J, Kim YH, Kim J, et al. YAP/TAZ regulates sprouting angiogenesis and vascular barrier maturation. J Clin Invest 2017;127:3441–3461.
30. Boopathy GTK, Hong W. Role of Hippo pathway-YAP/TAZ signaling in angiogenesis. Front Cell Dev Biol 2019;7:49.
31. Makino Y, Hikita H, Kato S, et al. STAT3 is activated by CTGF-mediated tumor-stroma cross talk to promote HCC progression. Cell Mol Gastroenterol Hepatol 2023; 15:99–119.
32. Pi L, Robinson PM, Jorgensen M, et al. Connective tissue growth factor and integrin alphavbeta6: a new pair of regulators critical for ductular reaction and biliary fibrosis in mice. Hepatology 2015;61:678–691.
33. Gao R, Brigstock DR. Connective tissue growth factor (CCN2) induces adhesion of rat activated hepatic stellate cells by binding of its C-terminal domain to integrin alpha(v)beta(3) and heparan sulfate proteoglycan. J Biol Chem 2004;279:8848–8855.
34. Miyazaki O, Kurashita S, Fukamachi I, et al. Subtraction method for determination of N-terminal connective tissue growth factor. Ann Clin Biochem 2010; 47:205–211.
35. Jin S, Guerrero-Juarez CF, Zhang L, et al. Inference and analysis of cell-cell communication using CellChat. Nat Commun 2021;12:1088.
36. Chen Z, Zhang N, Chu HY, et al. Connective tissue growth factor: from molecular understandings to drug discovery. Front Cell Dev Biol 2020;8:593269.
37. Atsumi T, Singh R, Sabharwal L, et al. Inflammation amplifier, a new paradigm in cancer biology. Cancer Res 2014;74:8–14.

38. Nguyen-Lefebvre AT, Selzner N, Wrana JL, et al. The hippo pathway: a master regulator of liver metabolism, regeneration, and disease. FASEB J 2021;35:e21570.
39. Salloum S, Jeyarajan AJ, Kruger AJ, et al. Fatty acids activate the transcriptional coactivator YAP1 to promote liver fibrosis via p38 mitogen-activated protein kinase. Cell Mol Gastroenterol Hepatol 2021;12:1297–1310.
40. Mannaerts I, Leite SB, Verhulst S, et al. The Hippo pathway effector YAP controls mouse hepatic stellate cell activation. J Hepatol 2015;63:679–688.
41. Totaro A, Panciera T, Piccolo S. YAP/TAZ upstream signals and downstream responses. Nat Cell Biol 2018; 20:888–899.
42. Ortega-Ribera M, Gibert-Ramos A, Abad-Jordà L, et al. Increased sinusoidal pressure impairs liver endothelial mechanosensing, uncovering novel biomarkers of portal hypertension. JHEP Rep 2023;5:100722.
43. Iwakiri Y, Trebicka J. Portal hypertension in cirrhosis: pathophysiological mechanisms and therapy. JHEP Rep 2021;3:100316.
44. Gan C, Yaqoob U, Lu J, et al. Liver sinusoidal endothelial cells contribute to portal hypertension through collagen type IV-driven sinusoidal remodeling. JCI Insight 2024;9: e174775.
45. Slack RJ, Macdonald SJF, Roper JA, et al. Emerging therapeutic opportunities for integrin inhibitors. Nat Rev Drug Discov 2022;21:60–78.
46. Shobaki N, Sato Y, Harashima H. Mixing lipids to manipulate the ionization status of lipid nanoparticles for specific tissue targeting. Int J Nanomedicine 2018; 13:8395–8410.
47. Hu P, Rychik J, Zhao J, et al. Single-cell multiomics guided mechanistic understanding of Fontan-associated liver disease. Sci Transl Med 2024;16:eadk6213.
48. Ma S, Habash NW, Dehankar MK, et al. Congestion enriches intra-hepatic macrophages through reverse zonation of CXCL9 in liver sinusoidal endothelial cells. Cell Mol Gastroenterol Hepatol 2025;19:101475.

Received March 13, 2025. Accepted November 10, 2025.

Correspondence
Address correspondence to: Tetsuo Takehara, MD, PhD, Department of Gastroenterology and Hepatology, Graduate School of Medicine, The University of Osaka, 2–2 Yamadaoka, Suita, Osaka 565–0871, Japan. e-mail: takehara@gh.med.osaka-u.ac.jp.

Acknowledgments
We gratefully acknowledge Prof Seiji Takashima (Department of Medical Biochemistry, Graduate School of Medicine/Frontier Biosciences, Osaka University, Osaka, Japan) for providing the hydrostatic pressure loading device and Tomoaki Mizuno (Center for Medical Research and Education, Graduate School of Medicine, Osaka University) for sample preparation for electron microscopy.

CRediT Authorship Contributions
Seiya Kato, MD (Conceptualization: Lead; Data curation: Lead; Formal analysis: Lead; Investigation: Lead; Methodology: Lead; Project administration: Equal; Resources: Equal; Software: Lead; Validation: Lead; Visualization: Lead; Writing – original draft: Lead)
Hayato Hikita, MD, PhD (Conceptualization: Equal; Data curation: Equal; Formal analysis: Equal; Funding acquisition: Lead; Methodology: Equal; Project administration: Equal; Supervision: Equal; Writing – review & editing: Equal)
Osamu Tsukamoto, MD, PhD (Data curation: Supporting; Formal analysis: Supporting; Methodology: Equal)
Katsuhiko Sato, MD, PhD (Data curation: Supporting; Formal analysis: Supporting; Methodology: Supporting)
Kohei Kamizono, MD (Data curation: Supporting; Formal analysis: Supporting)
Yoichi Sasaki, MD (Data curation: Supporting; Formal analysis: Supporting)
Kenji Fukumoto, MD (Data curation: Supporting; Formal analysis: Supporting)
Yuta Myojin, MD, PhD (Data curation: Supporting; Validation: Supporting)
Kazuhiro Murai, MD, PhD (Data curation: Supporting; Formal analysis: Supporting)
Yuki Tahata, MD, PhD (Formal analysis: Supporting; Resources: Equal)
Yuki Makino, MD, PhD (Data curation: Supporting; Validation: Supporting)
Yoshinobu Saito, MD, PhD (Methodology: Equal)
Takahiro Kodama, MD, PhD (Methodology: Equal)
Daisuke Motooka, MD, PhD (Data curation: Supporting; Software: Equal)
Shogo Kobayashi, MD, PhD (Resources: Equal)
Hideki Yokoi, MD, PhD (Resources: Equal)
Masashi Mukoyama, MD, PhD (Resources: Equal)
Yoshiaki Kubota, MD, PhD (Resources: Equal)
Tomohide Tatsumi, MD, PhD (Resources: Equal)
Hidetoshi Eguchi, MD, PhD (Resources: Equal)
Tetsuo Takehara, MD, PhD (Conceptualization: Equal; Data curation: Equal; Formal analysis: Equal; Funding acquisition: Equal; Methodology: Equal; Project administration: Lead; Supervision: Lead; Writing – review & editing: Lead)

Conflicts of interest
The authors disclose no conflicts.

Funding
This work was supported by the Japan Agency for Medical Research and Development (AMED), Grant Number JP24fk0210137 (H. Hikita).

Data Availability
There are no restrictions on data availability. All data supporting the findings of this study are available within the main text and supplementary information. The law and processed data will be available at Gene Expression Omnibus (GEO): the RNA-seq data of mLSECs subjected to HPS (GSE291322), the scRNA-seq data of murine livers after pIVCL (GSE291326), the scRNA-seq data of murine livers treated with CWHM-12 after pIVCL (GSE305630), the scRNA-seq data of the livers from endothelial cell–specific CTGF-KO mice after pIVCL (GSE305482), the scRNA-seq data of murine livers treated with carbon tetrachloride (GSE305772), the scRNA-seq data of human FALD and normal livers (GSE291325), and the spatial transcriptomic data of human FALD and normal livers (GSE306111).